Contrib Mineral Petrol (2005) 149: 266–275
DOI 10.1007/s00410-005-0654-y

ORIGINAL PAPER

M. Mellini · C. Rumori · C. Viti

Hydrothermally reset magmatic spinels in retrograde serpentinites: formation of "ferritchromit" rims and chlorite aureoles

Received: 24 July 2004 / Accepted: 2 February 2005 / Published online: 9 March 2005

Abstract Serpentinized harzburgites from southern Tuscany (Italy) host different kinds of spinels: (a) relic, magmatic Al-spinels, (b) hydrothermally altered spinels, occurring as "ferritchromit" rims, (c) syn- and post-serpentinization magnetites. The composition of relic Al-spinels suggests 5–15% partial melting of a fertile, spinel lherzolite. After the main serpentinization, Al-spinels are progressively replaced by ferritchromit rims by a dissolution–recrystallization process. Transmission electron microscopic investigation shows that ferritchromit actually consists of a complex, nanometric association of Cr-magnetite ($Mg_{0.03}$ $Fe^{2+}_{0.97}$ $Al_{0.11}$ $Cr_{0.89}$ $Fe^{3+}_{1.00}$ O_4), chlorite and lizardite, with $(001)_{chl/liz}$ always parallel to $(111)_{Cr\text{-}mag}$. Mg and Al, released during the Al-spinel → ferritchromit replacement, interact with mesh-textured serpentine, giving rise to chloritic aureoles (i.e., randomly intergrown chlorite, lizardite and "septechlorite") that overgrow and postdate mesh textures.

Introduction

Serpentinization and deserpentinization processes recycle matter from the mantle to the crust and back to the mantle, through the states of fertile peridotite, residual harzburgite, serpentinized oceanic crust, subducted and obducted ophiolites. Because they contain traces of that history, serpentinites deserve detailed study, notwithstanding the difficult task of deriving information from these complex rocks. Results are easily transferred from the outcrop to the global scale, because of the repetitive patterns of serpentinite evolution (at least, under common geodynamic settings).

These traces may be extracted by spatially resolved tools (i.e., textural analysis and microanalysis, at any scale) more easily than by bulk data. For this reason, we previously applied microanalytical and spectroscopic techniques to serpentinites from Internal Ligurid (IL) Units, specifically from Elba Island (Viti and Mellini 1996, 1997, 1998; Fuchs et al. 1998; Mellini et al. 2002) and southern Tuscany (Anselmi et al. 2000; Rumori et al. 2004; Viti et al. submitted).

We describe here the presence of different spinel generations in IL serpentinites and the retrograde transformations from magmatic spinel to "ferritchromit" rims (e.g., Kimball 1990) and chloritic aureoles. Spinels, refractory and resistant to alteration, are reliable petrogenetic indicators (Barnes and Roeder 2001), capable of recording the magmatic history by which a fertile spinel lherzolite undergoes partial melting, producing basalt melt and residual harzburgites (Hellebrand et al. 2001). However, magmatic spinels may re-equilibrate with surrounding silicates during prolonged cooling and metamorphism (Kimball 1990), thus possibly producing swarms of spinel compositions that have no bearing upon the magmatic history.

The study of hydrothermal spinel alteration offers a clue on the origin of chlorite too. Namely, altered spinels induce short-range metasomatic exchanges that feed transformation of lizardite to chlorite (Golding and Bayliss 1968; Onyeagocha 1974).

Geological setting

The specimens have been selected within a suite of serpentinites belonging to the ophiolites outcropping in Northern Apennine (NA) and southern Tuscany (ST). They are usually subdivided in Internal Liguride (IL) and External Liguride Units (EL), approximately with harzburgitic and lherzolitic compositions, respectively

Editorial Responsibility: I. Parsons

M. Mellini · C. Rumori · C. Viti (✉)
Dipartimento di Scienze della Terra, Università di Siena,
Via Laterina 8, 53100 Siena, Italy
E-mail: vitic@unisi.it
Tel.: +39-577-233830
Fax: +39-577-233938

(Hébert et al. 1989; Piccardo et al. 1990). The Ligurian peridotites, rather than representing a mature ocean, represent early oceanization through passive lithosphere extension, as presently occurring in embryonic oceans or at passive margins (Rampone and Piccardo 2000; Tribuzio et al. 2000; Piccardo et al. 2002). In particular, IL ophiolites would correspond to the late stage of the Ligurian–Piedmontese ocean spreading. Southernmost IL ophiolites have been sometimes named as ST ophiolites, although their specific paleogeographic domain, if different, has not been accurately determined (Tribuzio et al. 2000). For this reason, we will include ST in IL serpentinites. In contrast with Alpine and Western Ligurian ophiolites (Hébert et al. 1989; Scambelluri et al. 1995), after ocean-floor metamorphism NA and ST serpentinites escaped the tectonometamorphic events that elsewhere produced major deformation and prograde metamorphism. Therefore, they offer a favourable setting for the study of early reactions.

Serpentinized IL peridotites outcrop in Elba Island (Viti and Mellini 1998), Monti Livornesi and Murlo (Anselmi et al. 2000), hereafter labelled as E, ML and M, respectively. Most of them are harzburgites, with retrograde pseudomorphic textures (Wicks and Whittaker 1977). They occur also in the nearby Val di Cecina (VC), as outcrops some hundreds of meters wide. From site to site, VC serpentinites may differ in amount of deformation, fracturing, serpentinization extent and weathering. Most of them occur as fresh, unaltered blocks (some meters in size) surrounded by deformed, weathered zones.

XRF and XRPD data

Whole-rock analyses were performed by a Philips Magix-Pro X-ray fluorescence (XRF) spectrometer. XRF results for selected samples (VC33, VC23, E7 and VC17, in order of increasing Al-spinel alteration) are reported in Table 1. Fe^{2+}/Fe^{3+} was determined by titrimetry. Compositions, internally homogeneous and in close agreement with average data for M, E and ML serpentinites (Viti and Mellini 1998; Anselmi et al. 2000; Rumori et al. 2004), indicate a common harzburgitic protolith. Despite the different geodynamical settings, similar compositions have also been reported for mantle peridotites from ocean basins (Bonatti and Michael 1989). X-ray powder diffraction patterns (XRPD) of whole-rock serpentinites were recorded by an automated Philips PW1710 Bragg-Brentano diffractometer, equipped with post-diffraction monochromator, using Cu Kα radiation. All samples contain lizardite and minor magnetite; a frequent peak at 14 Å suggests chlorite, as already observed in Anselmi et al. (2000). In samples VC33 and VC23, the $(220)_{spl}$ reflection was split, leading us to identify two different, coexisting spinels (i.e., magnetite and Al-rich spinel, having $d_{220} =$ 2.969 and 2.859 Å, respectively). In contrast, VC17 and E7 gave only magnetite. The occurrence of two spinels (chromite, at 8.287 Å, and "ferritchromit", at 8.38–8.39 Å) together with chlorite was previously reported by Beeson and Jackson (1969) from altered portions of the Stillwater Complex chromitites.

Microtextural features

The new specimens from VC serpentinites display pseudomorphic retrograde textures (meshes and bastites), similar to other IL serpentinites (Viti and Mellini 1998; Anselmi et al. 2000). Serpentinization extent is variable, even within the same outcrop, with relic Al-spinel, olivine, ortho- and clinopyroxenes. Serpentine replaces the peridotitic minerals, completely or forming rims around olivine and lamellae parallel to the pyroxene cleavages. Two-pyroxene geothermometry gives

Table 1 Whole-rock XRF data (major elements, wt% oxides; minor elements, ppm;) of selected serpentinites from Val di Cecina and Elba, in order of increasing Al-spinel alteration

Average values for the Val di Cecina (*av.VC*), Murlo (*av.M*), Elba (*av.E*) and Monti Livornesi (*av. ML*) samples are also reported for comparison. *ND* not determined

	VC33	VC23	E7	VC17	av.VC	av.M	av.E	av.ML
SiO_2	39.56	39.53	38.96	39.52	39.54	38.03	38.88	38.88
TiO_2	0.08	0.08	0.01	0.05	0.06	0.05	0.04	0.05
Al_2O_3	1.63	1.58	0.85	0.96	1.31	1.47	1.44	1.55
Fe_2O_3	3.63	3.41	5.54	4.35	4.24	4.82	4.92	6.12
FeO	3.75	2.92	1.68	2.66	2.58	2.45	1.76	1.18
MnO	0.12	0.12	0.09	0.10	0.11	0.10	0.10	0.10
MgO	37.73	39.12	40.82	39.91	39.32	40.20	39.83	39.46
CaO	0.55	1.07	0.02	0.02	0.66	0.09	1.18	0.32
Na_2O	0.11	0.06	0.02	0.07	0.08	0.02	0.02	0.03
P_2O_5	0.01	0.00	0.00	0.00	0.00	0.00	0.01	0.00
LOI	12.84	12.10	12.01	12.36	12.10	12.77	11.83	12.33
Cl	512	521	221	388	399	326	347	414
V	55	56	15	57	59	57	57	58
Cr	2,354	2,212	1,169	2,691	2,383	2,648	2,134	2,198
Co	95	99	85	112	101	101	89	92
Ni	2,142	2,205	2,611	2,708	2,274	2,363	1,877	2,114
Cu	25	23	9	34	21	ND	ND	ND
Zn	48	53	22	45	45	37	48	38
Pb	15	18	7	17	14	15	14	15

equilibration temperatures of 1,240–1,051°C, followed by subsolidus cpx–opx exsolution at slightly lower T (1,145–1,025°C; Viti et al. submitted). Magnetite and hydrogarnet are always present. Pseudomorphic textures may be cut by late veins of fibrous-serpentine.

Different spinels occur in retrograde serpentinites: (a) relic, magmatic Al-spinels; (b) their alteration products (ferritchromit rims); (c) syn-serpentinization metamorphic magnetites and recrystallized post-serpentinization magnetites. Relic Al-spinels occur as fractured crystals with lobate contours. Amount and size (from 50 μm to 5 mm) are variable. Cores are yellow to deep-red, often surrounded by opaque rims that recall the highly reflective ferritchromit rims around chromites described elsewhere (e.g., Kimball 1990).

Ferritchromit rims are usually surrounded by irregular, colourless chloritic aureoles, up to 3 mm in size. Under crossed polars, chlorite shows polycrystalline extinction; the grains consist of fan-shaped sectors, with brown to deep-blue anomalous birefringence. Chlorite aureoles vary in size; the larger the opaque ferritchromit rim, the larger the chlorite aureole. Chlorite aureoles overgrow mesh textures, indicating that chlorite formed after main serpentinization. Similar chlorite aureoles have been previously reported for Elba serpentinites by Gianfagna et al. (1992).

Metamorphic magnetite mostly forms during olivine serpentinization. Thus, magnetite often occurs in mesh textures, both at the rim/rim boundary and within the core, as elongated strings and euhedral crystals, respectively. It occurs also as strings along bastite cleavage, after pyroxene serpentinization.

Finally, serpentinites show several low-T, post-serpentinization features, the most evident being water-induced magnetite recrystallization. Dissolved at the rim/rim contact, magnetite overgrows pre-existing textures producing a magnetite felt, preferentially replacing most disordered serpentines (e.g., chaotic mesh cores, bastites and late, poorly crystalline serpentine veins). These felts produce centimetric magnetite segregations that confer the typical bright/dark contrast to the hand-specimen. Ca-rich hydrogarnets crystallize as late features, mostly on bastites (as ''boudins'' consisting of micrometric equant crystals), within chloritic aureole and in late serpentine veins. Finally, minor deformation may erase pseudomorphic textures, or create slip- and cross-chrysotile veins (e.g., Andreani et al. 2004).

SEM microtextures and mineral compositions

Scanning electron microscopy (SEM) was performed using a Philips XL30, operating at 20 kV and equipped with an EDAX-DX4 energy dispersive spectrometer (EDS). The spectrometer detects elements with atomic number greater than 6 (i.e., C). Counting rate was kept close to 2,200–2,300 counts per second over the whole energy spectrum. Analytical precision, checked by repeated analyses, was better than 0.5% for major elements and better than 20% relative for minor elements (i.e., those ranging from 0.3 wt% up to 3–5 wt%). Raw data were corrected using the ZAF procedure, based on silicate mineral standards.

Average SEM/EDS data for spinels (Table 2) and back-scattered electron (BSE) images indicate contamination of spinel by tightly intermixed layer silicates (chlorite and lizardite, see later). Therefore, atoms per formula unit contents were calculated after removal of the silica content, together with the magnesia and alumina contents required to form ideal $Mg_3Si_2O_5(OH)_4$ serpentine. A.p.f.u. are expressed on the basis of four oxygens; Fe^{2+}/Fe^{3+} was calculated to assure charge balance.

Table 2 SEM/EDS compositions for spinels in serpentinites from Val di Cecina and Elba Island (averages of at least five point analyses for specimen), in order of increasing Cr# = Cr/(Cr + Al)

	VC33	VC22	VC24	VC8	VC1	VC5	VC30	VC21	VC35	VC23	VC27	E7	E1	VC17
SiO_2	0.46	0.37	0.43	0.00	0.00	0.15	0.35	0.55	0.42	0.00	0.71	0.00	2.62	2.66
TiO_2	0.21	0.17	0.18	0.17	0.00	0.10	0.19	0.43	0.55	0.61	0.62	0.47	0.19	0.44
Al_2O_3	54.44	54.05	52.99	53.06	48.91	46.44	46.21	39.31	34.40	32.82	30.05	3.60	0.98	0.88
Cr_2O_3	12.99	13.54	14.41	15.66	20.58	22.28	21.72	26.76	29.71	32.62	34.89	22.65	10.40	25.31
FeO	10.75	11.11	11.49	10.64	11.74	12.57	11.88	16.82	19.83	17.71	18.97	67.90	80.46	62.57
MnO	0.11	0.15	0.13	0.08	0.00	0.08	0.09	0.16	0.22	0.14	0.32	1.88	1.83	6.28
MgO	20.93	20.47	20.25	20.29	18.77	18.31	19.43	15.80	14.72	15.92	14.24	3.29	3.36	1.29
CaO	0.11	0.14	0.12	0.11	0.00	0.07	0.12	0.16	0.16	0.17	0.21	0.21	0.16	0.58
Ti	0.00	0.00	0.00	0.00	0.00	0.00	0.00	0.01	0.01	0.01	0.01	0.01	0.00	0.01
Al	1.67	1.66	1.64	1.64	1.55	1.49	1.46	1.31	1.17	1.11	1.05	0.14	0.04	0.04
Cr	0.27	0.28	0.30	0.32	0.44	0.48	0.47	0.60	0.68	0.74	0.82	0.60	0.28	0.76
Fe^{3+}	0.05	0.05	0.05	0.03	0.02	0.03	0.06	0.07	0.13	0.12	0.11	1.24	1.67	1.17
Fe^{2+}	0.19	0.20	0.20	0.21	0.25	0.26	0.22	0.33	0.37	0.32	0.37	0.80	0.79	0.82
Mn	0.00	0.00	0.00	0.00	0.00	0.00	0.00	0.00	0.00	0.00	0.01	0.04	0.04	0.17
Mg	0.81	0.80	0.79	0.79	0.75	0.74	0.78	0.67	0.63	0.68	0.63	0.16	0.17	0.00
Ca	0.00	0.00	0.00	0.00	0.00	0.00	0.00	0.00	0.01	0.01	0.01	0.01	0.01	0.02
Cr/(Cr + Al)	0.14	0.14	0.15	0.17	0.22	0.24	0.24	0.31	0.37	0.40	0.44	0.81	0.88	0.95
Fe/(Mg + Fe)	0.19	0.20	0.21	0.21	0.25	0.26	0.22	0.33	0.37	0.32	0.37	0.83	0.82	1.00

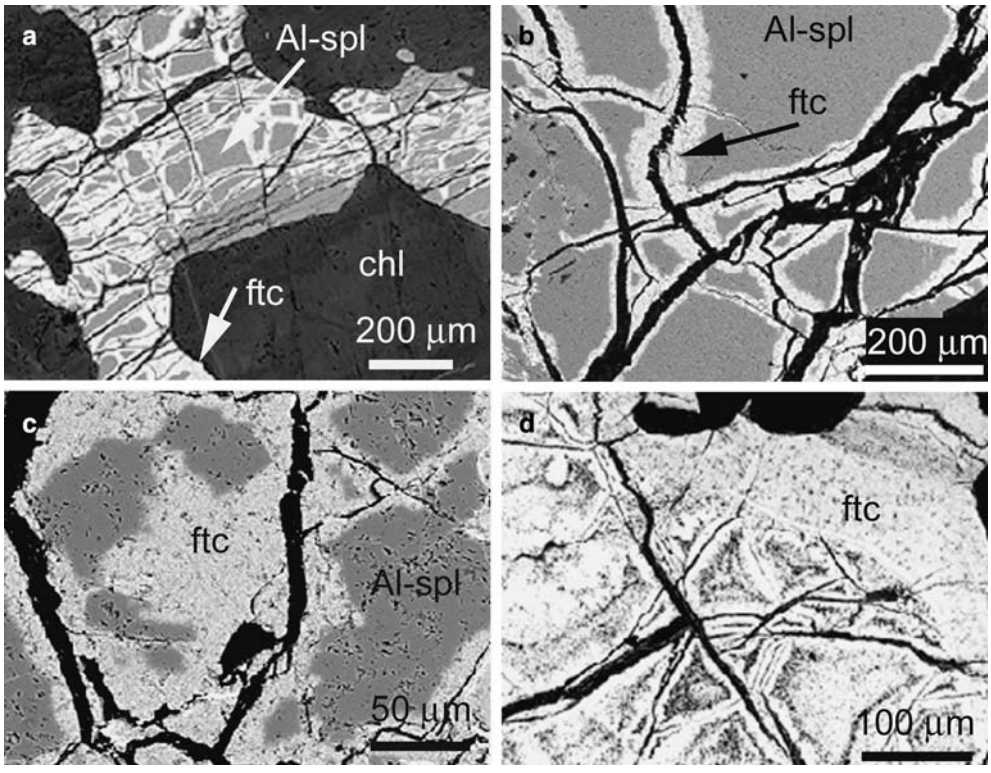

Fig. 1 SEM/BSE images of different Al-spinels, with variable alteration (increasing from **a** to **d**). **a** Anhedral Al-spinel crystal (*Al-spl*), affected by intense fracturing and partially replaced by ferritchromit (ftc, *bright rims*). Al-spinel is surrounded by a chloritic aureole (chl, *dark*). **b** Preserved, poorly fractured Al-spinel, partially replaced by thin ferritchromit rims. Fractures are filled by layer silicates. **c** Advanced Al-spinel – ferritchromit replacement. Note the irregular reaction front. **d** Completely replaced Al-spinel

Magmatic spinels and their alteration rims

In agreement with optical observations, relic Al-spinels occur as fractured crystals with anhedral contours, surrounded by chlorite aureoles (Fig. 1a). Replacement of Al-spinel (grey) by ferritchromit rims (bright) starts along fractures and progressively affects the Al-spinel sub-grains (Fig. 1b, c). Replacement extent is variable from sample to sample (e.g., increasing from Fig. 1a–1d). Whereas the outer grain contour is sharp, the Al-spinel – ferritchromit reaction boundary is irregular. Far from being homogeneous, the ferritchromit rim consists of submicrometric intergrown phases (i.e., Cr-magnetite and chlorite/lizardite, as detailed in the TEM section).

Chemical data sharply plot into two groups (Fig. 2) that mark the discontinuous change from magmatic Al-spinels to altered rims. Magmatic spinels, chemically homogeneous within the same sample, have Cr/(Cr + Al), hereafter Cr#, variable from sample to sample (0.14–0.44). In altered rims, Cr# is higher than 0.75. Thus, from primitive to altered spinels, compositions reequilibrate releasing magnesium and aluminum, and capturing chromium, ferrous and ferric iron, approximately by the exchange vector $Mg^{2+}_{-1}\,Fe^{2+}_{1}\,Al^{3+}_{-2}\,(Fe^{3+}, Cr)_2$.

Chlorite aureoles

Samples VC23, E7 and E1, with advanced ferritchromit replacement, were used to study the chemical variation through the chloritic aureole, from the inner contact with ferritchromit, up to the external contact with mesh-textured serpentine. Chemical data (recalculated on the basis of seven oxygens) range continuously from Al-rich chlorite to Al-poor lizardite compositions (Fig. 3). This cumulative trend does not correspond to an increasing distance from inner spinel; conversely, data, randomly distributed along the transects, suggest random lizardite–chlorite intermixing within the "chlorite aureole".

TEM observations

Transmission electron microscopic investigation was performed by a JEOL 2010, working at 200 kV and equipped with an ISIS-Oxford EDS spectrometer (see Rumori et al. 2004 for experimental details).

Different grids have been obtained for VC17, VC23 and VC33 samples, sampling Al-spinel → ferritchromit reaction boundaries and chloritic aureoles. Textures recall the optical and SEM observations, with four geochemical–mineralogical domains: (1) unreacted Al-spinel cores, (2) "porous" reacted Al-spinel rims, (3) ferritchromit assemblages (consisting of a complex Cr-magnetite + lizardite and chlorite association), and (4) chlorite and lizardite random intergrowths, forming chloritic aureoles and extending up to the serpentine meshes. Overall observations indicate that Al-spinel undergoes dissolution, giving rise to the ferritchromit rim; the new spinel retains Cr and Fe (Cr-magnetite), whereas Al and Mg are fixed in the coexisting layer silicates (chlorite/lizardite). Excess Al reacts further with serpentine in mesh textures, producing chloritic aureoles.

Unreacted Al-spinel is ordered and homogeneous, with sharp, intense reflections in selected area electron diffraction patterns. Measured *d*-spacings give a unit-cell parameter of 8.32 Å, calculated using carefully calibrated camera length values. Average TEM/EDS composition (a.p.f.u.) for sample VC33 is $Mg_{0.69}\ Fe^{2+}{}_{0.31}\ Al_{1.57}\ Cr_{0.40}\ Fe^{3+}{}_{0.02}\ O_4$. By comparison with the corresponding SEM/EDS data (collected close to spinel cores), TEM/EDS data (collected close to spinel rims) are (Al, Mg)-depleted and (Fe, Cr)-enriched.

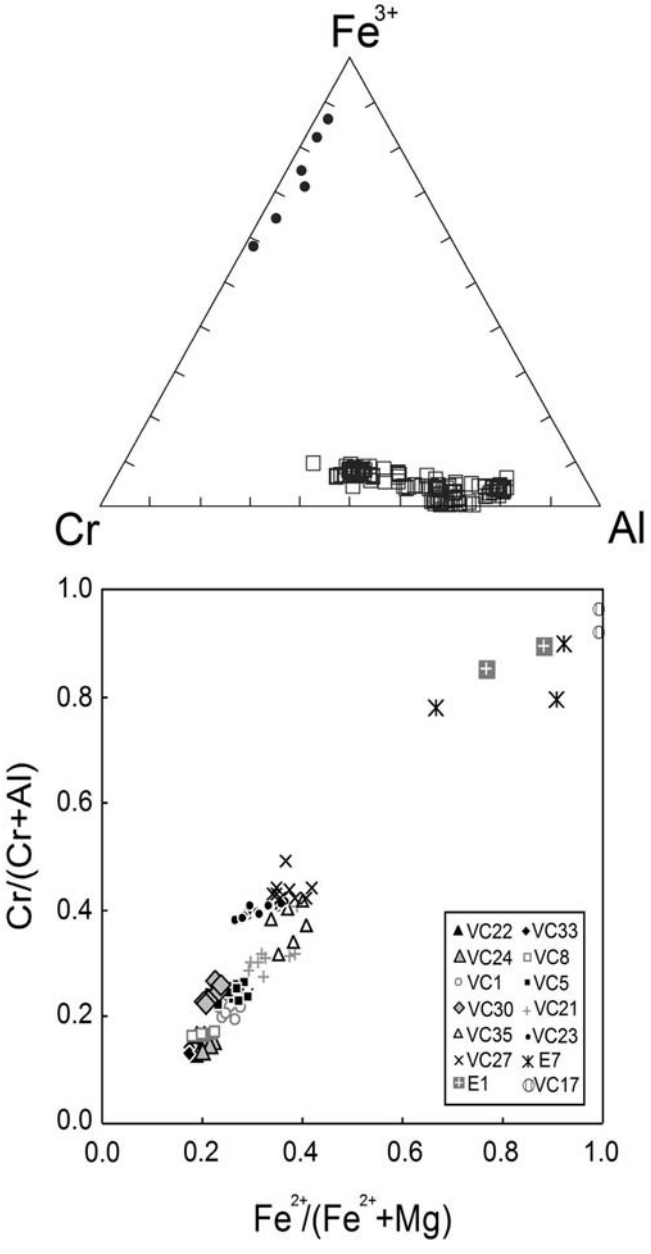

Fig. 2 **a** Ternary plot of trivalent cation contents in Al-spinels and ferritchromit rims, showing the sharp separation between magmatic (*bottom*) and altered, Fe-enriched (*top*) spinels. **b** Cr/(Cr + Al) vs. $Fe^{2+}/(Fe^{2+}$ + Mg) diagram for VC and E samples, showing intra-sample homogeneity and inter-sample variability

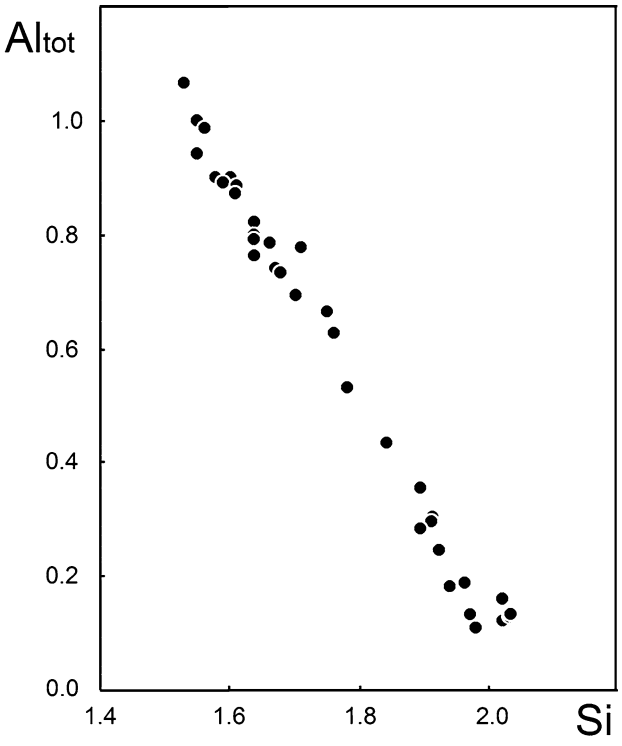

Fig. 3 Al_{tot} vs. Si contents in chloritic aureoles (SEM/EDS data, on the basis of seven oxygens). Compositional trend does not correspond to any textural zoning (i.e., the ideal transect from inner boundary with ferritchromit to outer boundary with mesh-textured serpentine)

Close to the reaction front, spinel becomes "porous", hosting nanometric anhedral voids (Fig. 4a). The transition from unreacted to "porous" spinel rim and ferritchromit is gradual, with irregular embayed boundaries (Fig. 4b). The amount and size of these voids are variable, becoming progressively more abundant towards the ferritchromit rim. The overall thickness of the "porous" spinel rim reaches ~1 μm. The presence of poorly crystalline, amorphous material within the voids suggests dissolution of the enclosing Al-spinel. We wonder whether voids still contain any fluid within the unthinned specimens.

The ferritchromit rim actually consists of intergrown euhedral dark grains and low-contrast material. Dark grains are Cr-magnetite ($Mg_{0.03}\ Fe^{2+}{}_{0.97}\ Al_{0.11}\ Cr_{0.89}\ Fe^{3+}{}_{1.00}\ O_4$, as average TEM/EDS composition); the low-contrast material corresponds to intermixed lizardite and chlorite layers. SAED patterns from wide areas (thus sampling several Cr-magnetite grains and lizardite/chlorite intergrowths) reveal that all Cr-magnetite grains share common orientation (i.e., they produce a single-crystal diffraction pattern), inherited from the nearby unreacted Al-spinel. Measured *d*-spacings for Cr-magnetite ($a = 8.46$ Å) are larger than for Al-spinel, due to the larger bivalent (Fe^{2+} vs. Mg) and trivalent (Fe^{3+} and Cr vs. Al) cations.

Both SAED patterns (Fig. 5a–b) and HR images (Fig. 5c–f) show close crystallographic and structural

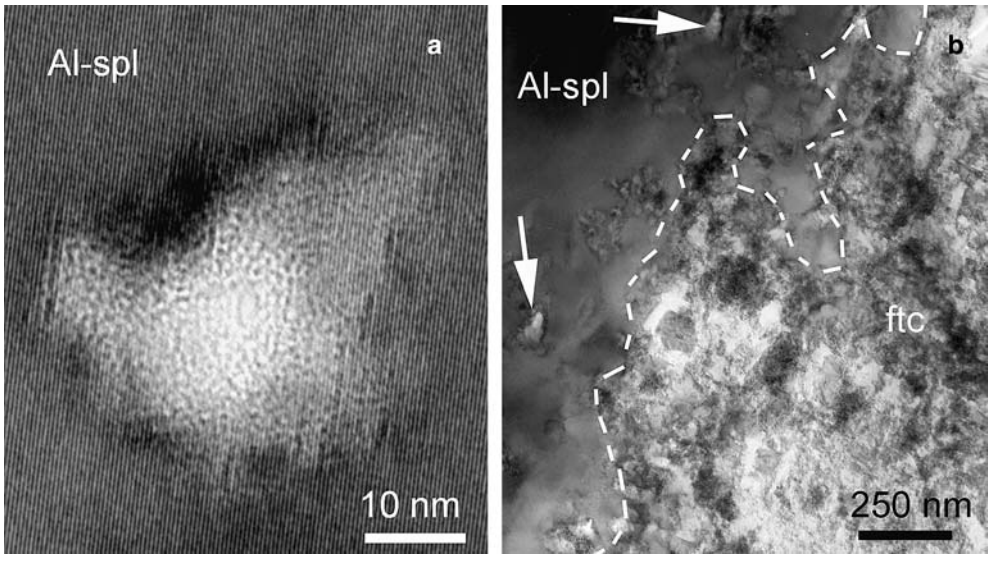

Fig. 4 **a** TEM image of pores within Al-spinel (*Al-spl*) close to the reaction front. Pores are partially filled by amorphous material. Note that the nearby Al-spinel structure is ordered and defect-free. **b** Low-magnification TEM image of the reaction front between Al-spl and ferritchromit rim (*ftc*). *Arrows* indicate pores within the reacting Al-spl. Ftc consists of a complex, multiphase association (i.e., *dark*- and *low-contrast phases*)

relationships between Cr-magnetite and the associated chlorite/lizardite, deriving from correspondence between $(111)_{Cr\text{-}mag}$ and $(001)_{chl/liz}$. Depending on crystal orientation (in particular, [112] and [110]), Cr-magnetites show elongated prismatic or equant, euhedral sections (Figs. 5c–e and d–f, respectively). Elongated grains are 5– 70 nm wide and 5–200 nm long (typically 20×100 nm), whereas equant grains vary from less than 5 nm up to 200 nm. Figure 5c and e shows $(001)_{chl/liz}$ parallel to spinel elongation (namely to $(111)_{Cr\text{-}mag}$). Figure 5d shows $(001)_{chl/liz}$ in two different orientations, parallel to $(111)_{Cr\text{-}mag}$ and to the symmetry-equivalent $(111)_{Cr\text{-}magnetite}$. Figure 5f is an enlarged view of Fig. 5d, showing the fine scale of the Cr-magnetite – chlorite/lizardite intergrowth, with $(001)_{chl/liz}$ parallel to $(111)_{Cr\text{-}mag}$. Similar close relationships between $(001)_{layer\ silicates}$ and $(111)_{spinel}$ have been previously observed during replacement of magnetite for annite; they have been already interpreted as preferred contact planes, namely as an epitaxy deriving from shared close-packed oxygens planes (Viti et al. 2004).

Chloritic aureoles consist of lizardite and chlorite, occurring either as ordered 7 or 14 Å - packets and as disordered intergrowths often associated with poorly crystalline material (Fig. 6a). The size of the ordered packets is variable, with largest crystals up to 0.1×1.0 μm in size. Most probably they are responsible for the lamellar texture and the anomalous birefringence observed in optical microscopy. Lamellae are preferentially iso-oriented, even though low-angle or random orientations also occur. TEM/EDS data range from Al-poor lizardite to Al-rich chlorite, with a continuous range of intermediate compositions (as already shown for SEM/EDS data in Fig. 3). Different kinds of [010] SAED patterns have been collected: 14 Å chlorite-like patterns with limited c* streaking (Fig. 6b); 7 Å, lizardite-like patterns with limited c* streaking (Fig. 6c); disordered 7 + 14 Å patterns with relevant c* streaking (Fig. 6d). In the last case, *00l* reflections with $l = 2n$ are sharp, whereas those with $l = 2n + 1$ display major streaking along c*. Surprisingly, there is no correspondence between SAED patterns and EDS compositions; in particular, lamellae with 7 Å periodicity along c* may give either Al-poor lizardite compositions or Al-rich chlorite-like compositions. Similar 7 Å lamellae with chloritic composition have been often called "septechlorite" (e.g., Cho and Fawcett 1986).

Discussion

For a long time, spinels have been considered as petrogenetic indicators, capable of conveying information about magmatic features (melt composition, melting degree and crystallization pressure). However, common hydrothermal alteration (Kimball 1990) results in increasing Cr# and Fe#. Therefore, in absence of detailed mineralogical and petrographic control, spinel compositions should not be interpreted uniquely in terms of igneous processes.

Actually, three different spinel compositions have been distinguished within the IL serpentinites:

- Magmatic Al-spinels, occurring as rounded anhedral grains, more or less preserved
- Hydrothermally altered spinels (ferritchromit rims); rather than a single phase, they consist of a complex association of Cr-magnetite + chlorite/lizardite; they are typically surrounded by chlorite aureoles
- Metamorphic, syn-serpentinization magnetites, occurring in mesh textures, at rim/rim boundaries and within mesh cores.

Each of these spinels conveys information about different steps of the peridotite evolution, as henceafter reported in detail.

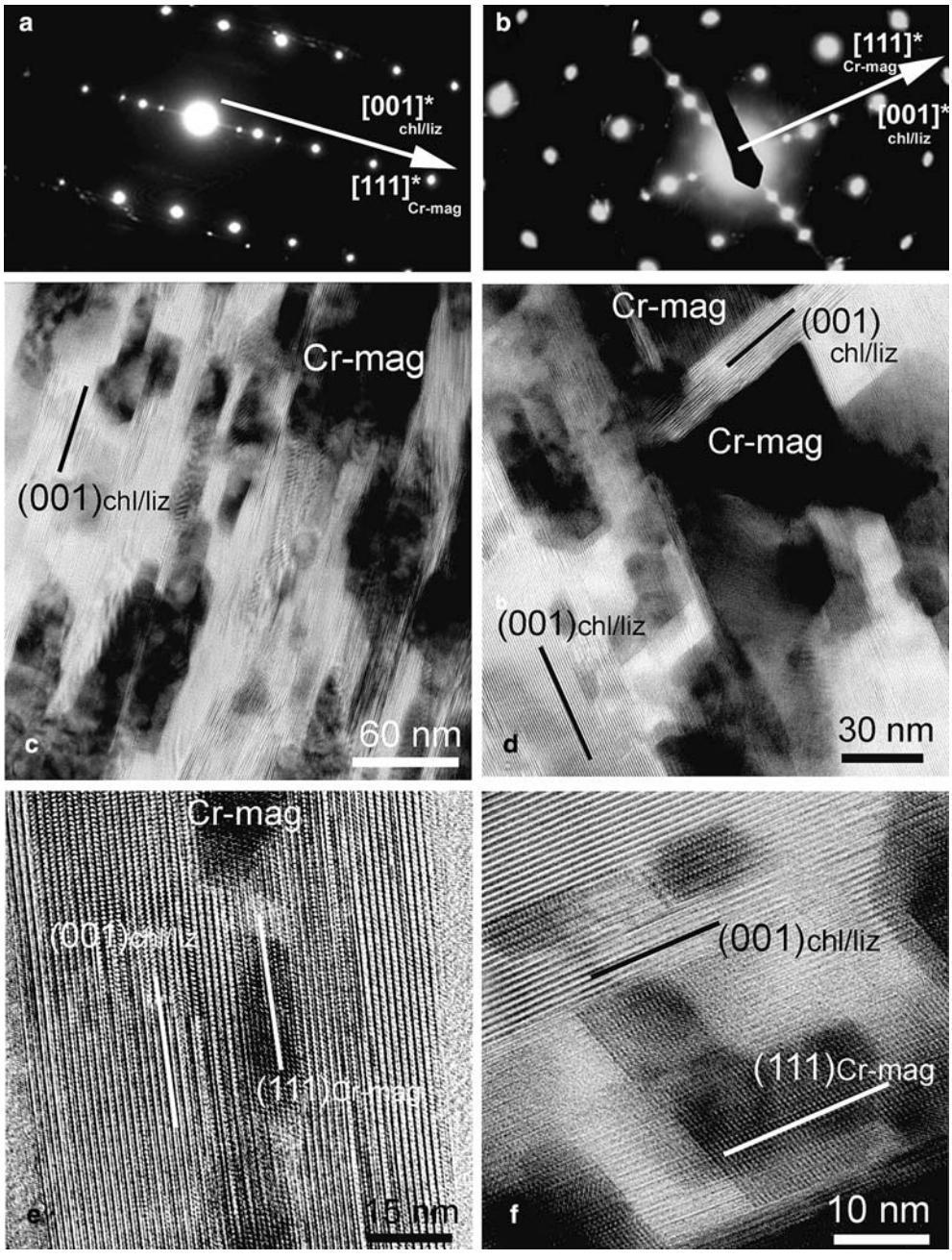

Fig. 5 TEM images of the ferritchromit assemblage, consisting of Cr-magnetites (Cr-mag) and chlorite/lizardite (*chl*/*liz*). **a, b** [112] and [110] SAED patterns, showing epitaxial orientations between spinel and layer silicates. **c, e** [112] projections, showing elongated Cr-magnetite grains, associated with random chlorite/lizardite sequences. Grain elongation corresponds to $(111)_{Cr\text{-}mag}$, which is parallel to $(001)_{chl/liz}$. **d, f** [110] projections, showing euhedral Cr-magnetite grains, intermixed with chlorite and lizardite. As evident from Fig. 5d, $(001)_{chl/liz}$ is parallel to $(111)_{Cr\text{-}mag}$ and the symmetry-related magnetite faces at 71° from (111)

Magmatic Al-spinels

They frequently occur as relics in IL serpentinites, testifying to their derivation from a spinel lherzolite protolith, expected to be stable within the 10–20 kbar range (e.g., Haggerty 1991). By partial melting, this protolith produced a Mg- and Cr- enriched, Si-, Fe- and Al-depleted residual harzburgite. IL Al-spinels closely match the compositions of samples dredged from South Atlantic fractures zones (e.g., the Islas Orcadas and Shaka Fracture Zones; Kimball 1990) and of abyssal peridotites (Haggerty 1991), as well as the comprehensive tabulations of ocean-floor peridotites by Barnes and Roeder (2001).

Hellebrand et al. (2001) used Al-spinels as a quantitative melting indicator of mantle residues. By using the early, fresh spinel compositions (i.e., the Al-rich spinels of Table 2 and Fig. 2) and carefully avoiding hydrothermally altered spinels, we estimate a 5–15% partial melting for IL peridotites (Cr# between 0.2 and 0.4). These estimates match the values for common abyssal peridotites (e.g., 10% beneath global ocean ridges, according to Niu and Hékinian 1997), stressing the similarity between oceanic peridotites and IL ophiolites. In detail, we wonder whether the observed Cr–Al trend corresponds to original heterogeneity of the lherzolitic peridotites, or indicates locally different melting extents.

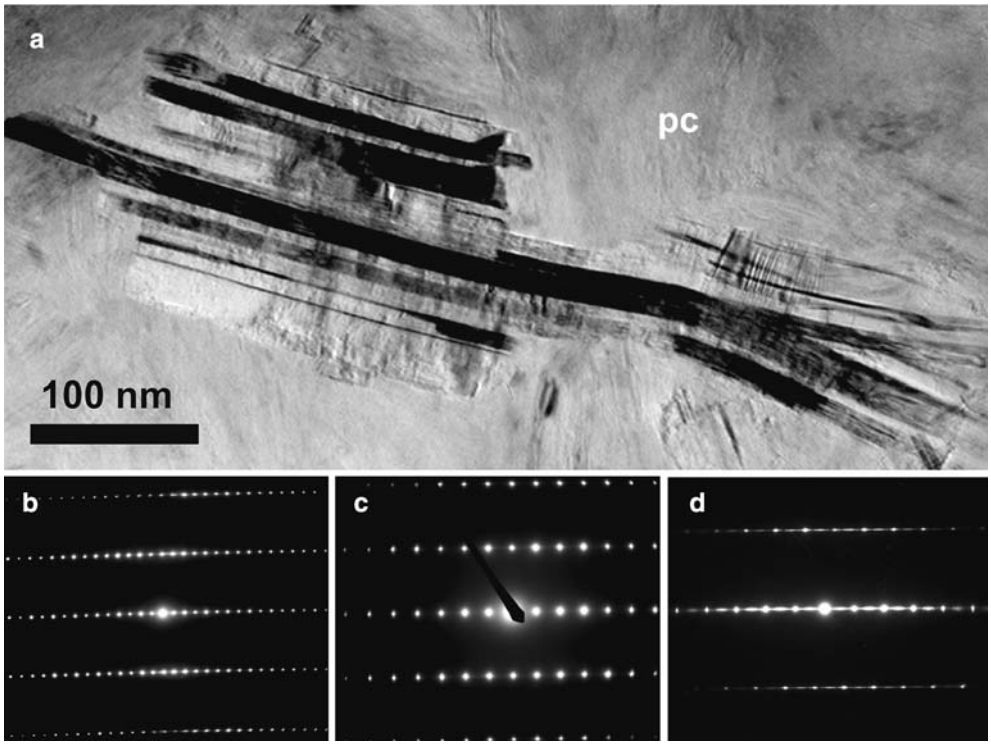

Fig. 6 **a** Low-magnification TEM image, showing the typical texture of chloritic aureoles. Chlorite and lizardite lamellae, often associated with poorly crystalline material (*pc*), occur in variable orientations. [010] SAED patterns of **b** 14 Å chlorite, with sharp reflections; **c** 7 Å lizardite, with sharp reflections; **d** disordered lizardite + chlorite lamella, with streaking along c*

Ferritchromit rims and chlorite aureoles

Altered spinels deviate from primitive Al-spinels, by sharp increase in Fe and Cr. The chemical change reflects hydrothermal metamorphic reactions between magmatic spinels and surrounding post-serpentinization silicate matrix. Al diffuses out of magmatic spinel, leaving behind a (Fe, Cr)-rich spinel (Cr-magnetite) and promoting the formation of chlorite aureoles.

The formation of chlorite through spinel alteration has been described by Kimball (1990) as a high *T* process (> 400°C) in presence of MgO- and SiO_2- rich fluids, according to the reaction

$$MgAl_2O_4 + 4MgO + 3SiO_2 + 4H_2O \rightarrow Mg_5Al\,Si_3Al\,O_{10}(OH)_8.$$

We agree with Kimball as regards the thermal environment of the hydrothermal reaction leading from magmatic spinels to chlorite. However, we suggest two stages of chlorite formation. The first one corresponds to the replacement of the primitive spinel by the ferritchromit melange. The second one affects the outer mesh serpentine, which is progressively transformed to a disordered chlorite/lizardite intergrowth. Thus, rather than a reaction of spinel with MgO- and SiO_2- rich fluids, we suggest that spinel reacted with already formed serpentines, as confirmed by textural evidence indicating that the chlorite aureole overgrew mesh-textured serpentines preserved elsewhere.

As evident from Fig. 2, during alteration spinel compositions evolve along the so-called Fe–Ti trend (Barnes and Roeder 2001; Spier and Filho 2001). In particular, the reaction mass balance requires transfer of the $MgAl_2O_4$ component from spinel to serpentine (thus producing $MgAl_2O_4$-depleted spinels and chlorite) under hydrothermal oxidizing conditions, according to reactions such as:

$$\underset{\text{Al - spinel}}{M\,Al_2O_4} + 1.5\,\underset{\text{serpentine}}{M_3Si_2O_5(OH)_4} + H_2O + 0.083O_2$$

$$\Rightarrow \underset{\text{chlorite}}{M_5Al\,Si_3Al\,O_{10}(OH)_8} + \underset{\text{Cr - magnetite}}{0.167M_3O_4}$$

with trivalent cations (iron and chromium) preferentially partitioned in magnetite. We stress that the formation of chlorite derives from Al-spinel alteration, with no need for the involvement of peridotitic plagioclase, as suggested elsewhere. Therefore, chloritic aureoles (or chloritic patches, as often reported) do not necessarily indicate plagioclase-bearing, lherzolitic protoliths.

Textures and compositions of IL serpentinites are similar to several other altered ultramafites. In the Coolac Serpentine Belt (Golding and Bayliss 1968) chlorite occurs as metasomatic zonal segregations, formed at pre-existing spinel–serpentine junctions, with chloritization influenced by aluminium released during chromite alteration. Similar reactions have been described also by Onyeagocha (1974) for the Twin Sisters dunite. Shen et al. (1988) observed that the Al- and Mg-depletion in ferritchromit was related to formation of interleaved chlorite and serpentine. Kimball (1990) reported pronounced Cr# zoning in spinels associated with aluminous phases such as hornblende or chlorite, and Fe# zoning in spinels associated only with serpen-

tine. Graham et al. (2001) associated fracturing and late-stage fluid migration in podiform chromitite with formation of clinochlore and uvarovite-grossular microcrystals in fractures and cavities. In particular, the presence of a two-step alteration process has been stressed for the Moa-Baracoa ophiolitic mass by Proenza et al. (1999); dunites and harzburgites are affected first by regional serpentinization, whereas a second alteration transforms chromite pods into ferrian chromite, accompanied by chloritization.

Magnetite

Compositions and textures of syn-serpentinization magnetite in IL serpentinites have been described by Rumori et al. (2004). In particular, magnetite forms at the same time as serpentine. Therefore, it forms before the re-equilibration of magmatic spinels to hydrothermally altered spinels. An important geochemical feature of the magnetite formation is the oxidation–reduction process leading to iron oxidation and hydrogen release, by the electron-transfer reaction:

$$Fe^{2+} + H_2O \rightarrow Fe^{3+} + OH^- + 0.5H_2.$$

This electronic pump is extremely important, because it is possibly responsible for the generation of important abiotic hydrocarbons (mostly methane, with minor more complex molecules), according to the Fischer-Tropsch transformation

$$4H_2 + CO_2 \rightarrow CH_4 + 2H_2O.$$

These hydrocarbons are known to produce important organic plumes in fracture zones (e.g., Mével 2003, and references therein), where they contribute food for oceanic life and, possibly, to gas-hydrates deposits.

A remark on the "septechlorite" term

The term "septechlorite" was introduced by Nelson and Roy (1954, 1958) to indicate a synthetic metastable trioctahedral 7 Å phase, extending between serpentine $Mg_3Si_2O_5(OH)_4$ and amesite $Mg_2AlSiAlO_5(OH)_4$, which transforms to chlorite only at $T > 450$°C. Velde (1973) synthesized "low-temperature 7 Å chlorites", separated in P–T space from 14 Å chlorite by a positive slope at $T = 450$–500°C. Cho and Fawcett (1986) called their product "7 Å chlorite", interpreted as a metastable precursor of 14 Å chlorite, recrystallized through a sluggish Ostwald process. Therefore, the terms "septechlorite" and "7 Å chlorite" have been commonly used, although never accepted in the official layer-silicates nomenclature. The improper name probably reflects the need of a specific term for an easily formed phase.

According to our electron diffraction and TEM/EDS data on natural serpentinites, Al leached from spinel is fixed within lizardite that conserves the 7 Å periodicity but approaches the chlorite composition, thus strongly recalling the features of "septechlorite". This intermediate phase later transforms to14 Å chlorite, visible also in the XRPD patterns. This case is related, but different, with respect to the fine-scale regular and irregular interstratifications of 7 and 14 Å phases (e.g., Banfield et al. 1994), to schemes for the 7 → 14 Å conversion given by Xu and Veblen (1996) and by Choo and Kim (2002).

We tentatively interpret our "septechlorite" as a disordered chlorite, with randomly distributed tetrahedral cations. Such a disordered distribution explains the easy nucleation, by introducing an entropy term capable of stabilizing the structure; at the same time, the enthalpy increase is negligible, because the structure has first-neighbour interactions similar to serpentine and chlorite. Equilibration to 14 Å chlorite, by atomic diffusion, would be a sluggish reaction, as suggested from the large activation energy of 90 ± 35 kcal/mol (Cho and Fawcett 1986). The driving force for recrystallization would be provided by optimized charge distribution, achieved obtaining alternating $[Mg_2\,Al\,(OH)_6]^+$ brucite-like sheets and $[Mg_3\,Si_3\,Al\,O_{10}\,(OH)_2]^-$ mica-like layers.

Conclusions

IL serpentinites formed by hydration of residual harzburgite, obtained by 5–15% partial melting of a fertile, spinel lherzolite, is estimated to occur at 1,240–1,051°C (Viti et al., submitted). Serpentinization occurred within the chlorite stability field (namely, at temperatures definitely higher than 350–400°C; Kimball 1990) forming mesh-textured serpentinites, with mesh cores and mesh rims decorated by syn-serpentinization magnetite.

After serpentinization, magmatic Al-spinels re-equilibrate within an oxidizing water-rich environment, exchanging the $MgAl_2O_4$ component with the surrounding mesh-textured serpentine. The reaction boundary is marked by the occurrence of a multiphase ferritchromit rim, consisting of intergrown lizardite, chlorite and Cr-magnetite. Outwards of the reaction boundary, wide chlorite aureoles form by metasomatic transformation of mesh serpentine, through a reaction intermediate having the properties of septechlorite (i.e., the chemical composition of chlorite and 7 Å c lattice parameter). Al-spinel destabilization and ferritchromit formation occurred after oceanic serpentinization, still within the chlorite stability field.

Acknowledgements Thanks are due to Alain Baronnet and Elena Belluso for their critical reviews of the manuscript.

References

Andreani M, Baronnet A, Boullier AM, Gratier JP (2004) A microstructural study of a "crack-seal" type serpentine vein using SEM and TEM techniques. Eur J Mineral 16:585–595

Anselmi B, Mellini M, Viti C (2000) Chlorine in the Elba, Monti Livornesi and Murlo serpentinites: evidence for sea-water interaction. Eur J Mineral 12:137–146

Banfield JF, Bailey SW, Barker WW (1994) Polysomatism, polytypism, defect microstructures and reaction mechanisms in regularly and randomly interstratified serpentine and chlorite. Contrib Mineral Petrol 117:137–150

Barnes SJ, Roeder PL (2001) The range of spinel composition in terrestrial mafic and ultramafic rocks. J Petrol 42:2279–2302

Beeson MH, Jackson ED (1969) Chemical composition of altered chromites from the Stillwater Complex, Montana. Am Mineral 54:1084–1100

Bonatti E, Michael PJ (1989) Mantle peridotites from continental rifts to ocean basins to subduction zones. Earth Planet Sci Lett 91:297–311

Cho M, Fawcett JJ (1986) A kinetic study of clinochlore and its high temperature equivalent forsterite-cordierite-spinel at 2 kbar water pressure. Am Mineral 71:68–77

Choo CO, Kim SJ (2002) Occurrence of chlorite and interstratified 7-Å phase in rhyodacitic tuff, south-eastern Korea, and implications for hydrothermal alteration conditions. Neues Jahrb Mineral Mh 2:49–67

Fuchs Y, Linares J, Mellini M (1998) Mössbauer and infrared spectrometry of lizardite-1T from Monte Fico, Elba. Phys Chem Miner 26:111–115

Gianfagna A, Grubessi O, Massera S (1992) Cr-rich-spinel chemistry of the serpentinites from the island of Elba, Tuscany, Italy: note I. Atti Soc Tosc Sci Nat Mem 99:175–194

Golding HG, Bayliss P (1968) Compact chlorite associated with lizardite from New South Wales, Australia. Mineral Mag 36:825–831

Graham IT, Franklin BJ, Marshall B (2001) Minerals in podiform chromitites-Tumut Serpentinite province, Southern NSW. Austr J Mineral 7:2–12

Haggerty SE (1991) Oxide mineralogy of the upper mantle. In: DH Lindsley (ed) Oxide minerals: petrologic and magnetic significance. Rev Mineral 25:355–416

Hébert R, Serri G, Hékinian R (1989) Mineral chemistry of ultramafic tectonites and ultramafic to gabbroic cumulates from the major oceanic basins and Northern Apennine ophiolites (Italy)-A comparison. Chem Geol 77:183–207

Hellebrand E, Snow E, Dick HJB, Hofmann AW (2001) Coupled major and trace elements as indicators of the extent of melting in mid-ocean-ridge peridotites. Nature 410:677–681

Kimball KL (1990) Effects of hydrothermal alteration on the composition of chromian spinels. Contrib Mineral Petrol 105:337–346

Mellini M, Fuchs Y, Viti C, Lemaire C, Linares J (2002) Insights into antigorite structure from Mössbauer and FTIR spectroscopies. Eur J Mineral 14:97–104

Mével C (2003) Serpentinization of abyssal peridotites at mid-ocean ridges. Comptes Rendus Geosci 335:825–852

Nelson BW, Roy R (1954) New data on the composition and identification of chlorites. In: Proceedings of the 2nd national conference on clays and clay minerals. Nat Res Council Publ 327:335–348

Nelson BW, Roy R (1958) Synthesis of chlorites and their structural and chemical constitutions. Am Mineral 43:707–725

Niu Y, Hékinian R (1997) Spreading-rate dependence of the extent of mantle melting beneath ocean ridges. Nature 385:326–329

Onyeagocha AC (1974) Alteration of chromite from the Twin Sisters Dunite, Washington. Am Mineral 59:608–612

Piccardo GB, Rampone E, Vannucci R (1990) Upper mantle evolution during continental rifting and ocean formation: evidences from peridotite bodies of the western Alpine-Northern Apennine system. Mém Soc Géol Fr 156:323–333

Piccardo GB, Rampone E, Romairone A (2002) Formation and composition of the oceanic lithosphere of the Ligurian Tethys: inferences from the Ligurian Ophiolites. Ofioliti 27:145–162

Proenza J, Solé J, Melgarejo JC (1999) Uvarovite in podiform chromitite: the Moa-Baracoa ophiolitic massif, Cuba. Can Mineral 37:679–690

Rampone E, Piccardo GB (2000) The ophiolite-oceanic lithosphere analogue: new insights from the Northern Apennines (Italy). Geol Soc Am Spec Pap 349:21–34

Rumori C, Mellini M, Viti C (2004) Oriented, not-topotactic olivine $\rightarrow$ serpentine replacement in mesh-textured, serpentinized peridotites. Eur J Mineral 16:731–741

Scambelluri M, Muntener O, Hermann J, Piccardo GB, Trommsdorff V (1995) Subduction of water into the mantle: history of an Alpine peridotite. Geology 23:459–462

Shen P, Hwang SL, Chu HT, Jeng RC (1988) STEM study of "ferritchromit" from the Heng-Chun chromitite. Am Mineral 73:383–388

Spier CA, Filho FF (2001) The chromite deposits of the Bacuri mafic-ultramafic layered complex, Guyana Shield, Amapà State, Brazil. Econ Geol 96:817–835

Tribuzio R, Tiepolo M, Vannucci R (2000) Evolution of gabbroic rocks of the Northern Apennine ophiolites (Italy): comparison with the lower oceanic crust from modern slow-spreading ridges. Geol Soc Am Spec Pap 349:129–138

Velde B (1973) Phase equilibria in the system MgO–Al_2O_3–SiO_2–H_2O: chlorites and associated minerals. Mineral Mag 39:297–312

Viti C, Mellini M (1996) Vein antigorites from Elba Island, Italy. Eur J Mineral 8:423–434

Viti C, Mellini M (1997) Contrasting chemical compositions in associated lizardite and chrysotile in veins from Elba, Italy. Eur J Mineral 9:585–596

Viti C, Mellini M (1998) Mesh textures and bastites in the Elba retrograde serpentinites. Eur J Mineral 10:1341–1359

Viti C, Di Vincenzo G, Mellini M (2004) Thermal transformations in laser-heated chloritized annite. Phys Chem Miner 31:92–101

Wicks FJ, Whittaker EJ (1977) Serpentine textures and serpentinization. Can Mineral 15:459–488

Xu H, Veblen DR (1996) Interstratification and other reaction microstructures in the chlorite-berthierine series. Contrib Mineral Petrol 124:291–301